Variational transition state theory based surface chemistry for the C_2H_6/H_2/O_2/Pt system

P. Kraus and R. P. Lindstedt[*]

Department of Mechanical Engineering, Imperial College, Exhibition Road,

London SW7 2AZ, UK

E-mail: p.lindstedt@imperial.ac.uk

Abstract

A reaction class-based framework for the development of heterogeneous mechanisms is applied to study the (partial) oxidation of ethane over platinum. The rate parameters for the surface chemistry were derived using a systematic application of variational transition state theory (VTST) for adsorption, desorption and Eley-Rideal reactions coupled with 2D collision theory for reactions occurring on the surface. The approach removes the need for the experimental determination of surface sticking coefficients and the associated major uncertainties. The barrier heights were determined using the unity bond index – quadratic exponential potential (UBI-QEP) method. The combined gas and surface phase chemistry was evaluated against independent data sets obtained from three experimental configurations. The associated 18 cases cover a wide range of residence times, stoichiometries ($0.1 < \phi < 10.4$) and inlet pressures (1 to 12 bar). The work highlights the generality of the VTST approach that is shown to outperform the customary sticking coefficient based methods for key aspects. A sensitivity analysis highlights the importance of the O_2 and CO adsorption pathways.

1 Introduction

The catalytic oxidation of hydrocarbons is a topic of significant interest. The partial oxida-
tion of ethane to ethylene[1–3] provides an example of extracting added value from traditional

---

[*]To whom correspondence should be addressed

feedstocks. The advantages of catalytic partial oxidation over the more common steam reforming include higher selectivity towards desired products[4] and lower energy requirements.[5] The available experimental data on ethane reactivity over platinum (Pt) generally falls into two categories: ethane hydrogenolysis, and oxidation. The C_2H_6–H_2/Pt system has been investigated in detail by Cortright *et al.*[6,7] and supported by the extensive density functional theory (DFT) study on small Pt clusters by Watwe.[8] More recently, Salciccioli *et al.*[9] explored the microkinetics of ethylene hydrogenation and ethane hydrogenolysis with accompanying DFT results on stepped surfaces presented by Chen and Vlachos.[10]

The C_2H_6–O_2–H_2/Pt system is less studied. Bodke *et al.*[1,11,12] experimentally investigated the effect of ceramic supports[11] on metal-catalysed partial oxidation with a focus on the C_2H_6–O_2/Pt system with varying amounts of hydrogen.[1,12] The data was used for a detailed microkinetic analysis and mechanism validation by Zerkle *et al.*[2] Vincent *et al.*[3,13] presented a set of short contact time reactor data with varying C_2H_6/O_2 ratios and inlet velocity,[3] reactor length and catalyst loading.[13] The results were used to validate a semi-automatic class-based method for developing surface reaction mechanisms and their coupling to the gas phase.[3] More recently, ethane oxidation was studied experimentally by Zheng *et al.*[14] An adjusted mechanism for fuel-lean ethane oxidation was proposed based on work of Zerkle *et al.*[2] and Deutschmann *et al.*[15]

Vincent *et al.*[3] defined four reaction classes (direct adsorption, adsorption on an adsorbate, surface reactions with adsorbed reactants and unimolecular surface reactions including desorption) and combined the unity bond index – quadratic exponential potential (UBI–QEP) method[16] with available data determined using DFT and/or experimental investigations to establish activation energies. The pre–exponential factors for adsorption processes were calculated using the collision theory approach formalised by Warnatz.[17] The latter requires the use of estimated or experimentally derived sticking coefficients, which can vary by orders of magnitude even for well studied reactions.[9] The prevalent lack of such data is a major obstacle to the derivation of reliable reaction mechanisms for surface processes.

Kraus and Lindstedt[18] presented a revised reaction-class based method and validated the resulting mechanism for catalytic combustion of hydrogen and syngas over Pt. The framework[18] addresses the dependency on external sticking coefficient data by using variational transition state theory (VTST) for adsorption and desorption processes. The VTST approach was combined with collision theory for the determination of pre–exponential terms for homogeneous surface reactions[3] and a systematic application of UBI–QEP for the determination of barrier heights.[16] It was shown that the approach removes major uncertainties for hydrogen and syngas oxidation over platinum. A reaction mechanism obtained using this method is here applied to (partial) ethane oxidation over platinum over a wide range of residence times, stoichiometries ($0.1 < \phi < 10.4$) and inlet pressures (1 to 12 bar) and comparisons made with the corresponding model based on sticking coefficients.[3] The work shows that the more general VTST approach can improve agreement with experimental data, while removing the need for the experimental determination of sticking coefficients. The approach also serves to identify key parameters where high accuracy *ab initio* methods may be required.

Experimental conditions

The experimental conditions used in the current work comprise 3 independent data sets featuring 18 cases. Zheng *et al.*[14] investigated catalytic oxidation of ethane under fuel-lean conditions in a platinum-coated duct reactor. A schematic of the experimental configuration is presented in Fig. 3. The conditions of the six representative cases chosen for validation are summarised in Table 1. The dataset spans a pressure range from 2 to 12 bar and equivalence ratios between 0.11 and 0.42. The selected conditions include cases with (E08–E09) and without (E02–E05) gas phase ignition. As the catalytic coating used in the duct reactor is non-porous,[14] the catalytic site density Γ is set to 27 μmol/m^2, corresponding to a close-packed monolayer of Pt.

Table 1: Experimental conditions for lean ethane oxidation.[14] Equivalence ratio φ, N_2/O_2 molar ratio, inlet velocity $U_{in}^{T_{in}}$, temperature of inlet gas T_{in}, temperature of the catalytic wall at inlet T_{in}^{W}, pressure P and the gas space velocity (GHSV) at 273 K and 1 bar. Catalytic site density $\Gamma = 27$ μmol/m^2 for all cases.

Case	φ	$\frac{N_2}{O_2}$	$U_{in}^{T_{in}}$ [m/s]	T_{in} [K]	T_{in}^{W} [K]	P [bar]	GHSV [1000/h]
E02	0.31	2.19	1.89	460	780	2	27
E03	0.41	3.78	0.90	454	810	4	26
E04	0.22	3.59	0.46	455	784	10	33
E05	0.11	0.60	0.39	461	741	12	33
E08	0.42	3.86	0.52	487	963	6	21
E09	0.40	3.88	0.51	505	1056	8	26

56   Fuel-rich conditions were investigated using a set of 12 partial catalytic oxidation cases

57 from Vincent *et al.*[3] and Bodke *et al.*[12] These investigations were performed in catalytic

58 foam reactors, shown schematically in Figs. 4 and 5. The conditions were chosen to inves-

59 tigate the trends in conversion ($\mathcal{C}$) and selectivity ($\mathcal{S}$) with variations in inlet stoichiometry

60 (V07–V12), residence time (V11, V13–V16) and hydrogen co-feed (B20–B23). An overview

61 of the conditions for all partial oxidation cases is presented in Table 2. For the cases of

62 Vincent *et al.*,[3] the platinum catalyst is well dispersed over the porous alumina support,

63 increasing the effective site density. Therefore, the value of site density (75 μmol/m^2) rec-

64 comended by the authors has been applied. As the characterisation data of the catalyst

65 used by Bodke *et al.*[12] is not available, the surface has been treated as a Pt monolayer,

66 corresponding to 27 μmol/m^2.

Gas phase and surface chemistries

68 The C_1–C_2 gas phase chemistry of Vincent *et al.*[3] was applied without modification, in-

69 cluding the corresponding thermochemical and transport data, to maintain consistency with

70 previous work.[13,18] The mechanism has previously been validated against a broad range of

71 homogeneous gas phase conditions including methane and ethane auto-ignition behaviour

Table 2: Experimental conditions of Vincent *et al.*[3] and Bodke *et al.*[12] for partial catalytic oxidation of ethane over a foam catalyst: H_2/O_2, C_2H_6/O_2 and N_2/O_2 mol ratios, the reference inlet velocity U_{in}^{273K}, the temperature of the inlet (reactant) gas T_{in}, the temperature of the reactor bath T_b, the catalytic site density Γ, the pressure P and the gas space velocity (GHSV) at 273 K and 1 bar.

Case	$\dfrac{H_2}{O_2}$	$\dfrac{C_2H_6}{O_2}$	$\dfrac{N_2}{O_2}$	U_{in}^{273K} [m/s]	T_{in} [K]	T_b [K]	Γ [μmol/m^2]	P [atm]	GHSV [1000/h]
V07	2.00	2.96	0.66	2.10	420	844	75	1.0	251
V09	2.00	2.42	0.60	2.10	421	867	75	1.0	251
V11	2.00	2.05	0.56	2.10	423	936	75	1.0	251
V12	2.00	1.90	0.54	2.10	424	981	75	1.0	251
V13	2.00	2.05	0.56	3.35	418	850	75	1.0	401
V14	2.00	2.05	0.56	4.18	408	806	75	1.0	500
V15	2.00	2.05	0.56	5.86	392	740	75	1.0	701
V16	2.00	2.05	0.56	6.72	383	681	75	1.0	804
B20	0.00	2.00	1.28	0.32	323	673	27	1.2	115
B21	1.00	2.00	1.28	0.32	323	673	27	1.2	115
B22	2.00	2.00	1.28	0.32	323	653	27	1.2	115
B23	3.00	2.00	1.28	0.32	323	633	27	1.2	115

and C_1–C_2 oxidation.[19–22] The mechanism comprises 44 gas phase species (N_g) and 271 reversible reactions.

Vincent *et al.*[3] combined collision theory and the UBI–QEP method of Shustorovich and Sellers[16] to systematically calculate rate parameters with energetics based on the heats of adsorption of reactants onto the catalyst (Q_R) and the total bond energies (E_R) of the reacting species as shown in Table 3. The approach was based on a "hybrid" data set[3,18] that included, when available, more accurate DFT and/or experimental determinations to compute model parameters. Such data are, however, typically limited for many surfaces. Accordingly, activation energies in the current mechanism were systematically calculated using UBI–QEP[16] in order to assess the robustness of such an approach. Overall, 239 forward or reverse barriers were replaced by values different by more than 20% from the values reported in the work of Kraus and Lindstedt.[18] Hence, potential refinement using barrier heights obtained from DFT is possible[3] as suggested by Shustorovich and Sellers.[16]

Table 3: Heats of adsorption on Pt and total bond energies for the VTST mechanism.[3] The adsorption modes of H(s), O(s) and COH(s) are calculated for a 3–atom hollow.

Species	$\mathbf{Q}_R$	E_R	Adsorption mode	Comment
	kJ/mol			
H(s)	255.0	–	H(s_3)	BOC–MP[23]
H$_2$(s)	26.8	431.24	H	BOC–MP[24]
O(s)	356.0	–	O(s_3)	BOC–MP[23]
O$_2$(s)	44.3	498.23	O	BOC–MP[24]
OH(s)	247.0	427.05	O	adjusted[3,24] from experiment[25,26]
OOH(s)	204.0	706.75	O – strong	UBI–QEP[16]
H$_2$O(s)	40.2	921.09	O	UBI–QEP[16]
H$_2$O$_2$(s_2)	27.1	1070.56	O–O	Vincent et $al.$[3]
C(s_3)	628.0	–	C	estimated[23,24,27]
CH(s_3)	407.0	339.13	C – strong	UBI–QEP[16]
CH$_2$(s_2)	283.0	761.99	C – strong	UBI–QEP[16]
CH$_3$(s)	159.0	1226.73	C – medium	UBI–QEP[16]
CCH(s)	287.0	1084.38	C	Vincent et $al.$[3]
CCH$_2$(s_2)	299.0	1457.01	C–C	Vincent et $al.$[3]
CCH$_2$(s_3)	149.0	1457.01	C–C + π	Vincent et $al.$[3]
CCH$_3$(s_3)	405.0	1569.29	C – strong	UBI–QEP[16]
CHCH$_2$(s)	184.0	1786.86	C–CH$_2$ + π	UBI–QEP[16]
CHCH$_2$(s_3)	129.0	1786.86	CH + CH$_2$	UBI–QEP[16]
CHCH$_3$(s_2)	294.0	1934.46	C – strong	UBI–QEP[3,27]
CH$_2$CH$_3$(s)	163.0	2411.60	C – medium	UBI–QEP[3,27]
C$_2$H$_2$(s_3)	134.0	1641.23	CH=CH + π	UBI–QEP[16]
C$_2$H$_4$(s)	68.0	2252.50	CH$_2$=CH$_2$ + π	UBI–QEP[16]
C$_2$H$_4$(s_2)	99.0	2252.50	CH$_2$–CH$_2$ di-σ	DFT[28]
C$_2$H$_6$(s_2)	36.1	2821.90	CH$_3$–CH$_3$	UBI–QEP[16]
CO(s_2)	134.0	1076.00	C	literature data[3,24,29]
CO$_2$(s)$_2$	15.1	1607.73	O	BOC–MP[24]
CHO(s)	167.0	1147.18	C – medium	UBI–QEP[3,27]
COH(s_3)	337.0	965.54	C(s_3)	Vincent et $al.$[3]
CHOH(s_2)	200.0	1300.41	C – medium	UBI–QEP[16]
COOH(s)	213.0	1646.03	C – strong	UBI–QEP[16]
CH$_2$O(s)	46.7	1511.43	O	UBI–QEP[16]
CH$_2$OH(s)	160.0	1637.00	C – medium	UBI–QEP[16]
CH$_3$O(s)	173.0	1603.54	O – strong	UBI–QEP[16]
CH$_3$OH(s)	44.1	2038.97	O	UBI–QEP[16]
CH$_4$	25.1	1666.34	–	adjusted[3,27] from Rhodium[30]

The heats of adsorption used to calculate the reaction barriers for the VTST mechanism are consistent with the values of Vincent *et al.*[3] In most cases, these result from the systematic application of the UBI–QEP method,[16] or its previous iteration, the bond order conservation – Morse potential (BOC–MP) method.[23] For $OH(s)$, $C_2H_4(s_2)$, $CO(s_2)$, CH_4 and $C(s_3)$ the values are obtained from other sources, such as DFT studies,[28] experimental determinations[25,26,30] or estimates.[23,24,27] For $H_2O_2(s_2)$, $CCH(s)$, $CCH_2(s_2)$, $CCH_2(s_3)$ and $COH(s_3)$ the determinations of Vincent *et al.*[3] are retained as shown in Table 3.

Possible surface chemistry pathways were initially determined using a combinatorial approach[31] followed by systematic reduction. For reasons of consistency, the pathways are retained from previous work.[18,32] The resulting reaction network is comprised of 35 adsorbed species (N_s) and 284 reversible reactions. The Arrhenius pre–exponentials and temperature dependencies (AT^β) for all reactions were obtained using the revised systematic VTST approach of Kraus and Lindstedt.[18] Overall, 249 pre–exponentials differ from the values proposed by Vincent *et al.*[3] by more than 20%. One of the main advantages of this framework is the ability to calculate pre-exponential terms for adsorption and desorption reactions in a manner that provides an improvement over classical TST[33] – especially for barrierless processes.[34] Furthermore, the contribution of the vibrational partition functions is systematically considered, with hindered rotors treated using the Pitzer–Gwinn method.[35] A comparison of the collision theory based approach of Vincent *et al.*[3] with the current VTST based method[18] can be found in Table 4. As shown, the 2D collision theory–based method of Vincent *et al.*[3] was used for homogeneous surface reactions with adsorption and desorption processes treated via the application of TST as described by Dumesic *et al.*[36] The definition of reaction classes is consistent with previous work.[3] All pre-exponential factors are further multiplied by Γ^{1-m}, where m indicates the total number of reactants and additional Pt sites involved in the reaction. Compared to the mechanism of Vincent *et al.*,[3] both E_A and AT^β were updated for 105 reactions, E_A for 134 reactions and AT^β for 144 reactions with 185 reactions unchanged. The mechanism is available in the SMM.

Table 4: Comparison of the treatment of adsorption, Eley-Rideal, desorption and surface rate constants in the collision theory based approach of Vincent *et al.*[3] and the current VTST approach.[18]

Reaction class[a]	Collision theory	Present work
Adsorption	$A = \frac{s_0}{x^x} A_{\text{Pt}} N_A \Gamma \overline{v_{2D}}$	$A = \frac{1}{x^x} \frac{k_B T}{h} \frac{Q_\ddagger}{Q_g}$
Eley-Rideal	$A = \frac{s_0}{x^x} A_{\text{Pt}} N_A \Gamma \overline{v_{2D}}$	$A = \frac{1}{x^x} \frac{k_B T}{h} \frac{Q_\ddagger}{Q_g} \frac{A_{\text{B}(s)}}{A_{\text{Pt}}}$
Bimolecular surface reaction Unimolecular + Pt site	$A = \frac{1}{3} \frac{2b}{x^x} N_A \Gamma^2 \overline{v_R}$	$A = \frac{1}{3} \frac{2b}{x^x} N_A \Gamma^2 \overline{v_R}$
Desorption	$A = \frac{k_B T}{h}$	$A = \frac{k_B T}{h} \frac{Q_\ddagger}{Q_s}$
Unimolecular	$A = \frac{1}{x^x} \frac{k_B T}{h}$	$A = \frac{1}{x^x} \frac{k_B T}{h}$

[a]Where x is the surface coordination of the adsorbing species, A_{Pt} and $A_{\text{B}(s)}$ the projected surface areas of Pt and species B, N_A Avogadros number, b the collision radius of the reacting pair, k_B and h the Boltzmann and Planck constants and Q_X the overall partition function of species X. The velocities $\overline{v_{2D}}$ and $\overline{v_R}$ correspond to the 2-dimensional Maxwellian and relative surface velocities respectively.

Partition functions for gas-phase and adsorbed species are required to determine the pre-exponential factors for adsorption and desorption processes. Based on the principle of microscopic reversibility, the adsorption transition state (TS, ‡) will be the same as the desorption TS, requiring a single additional partition function. The overall partition function of species X is defined as $Q_X = q_T q_V q_R q_E$, where q_T is the translational, q_V the vibrational, q_R the rotational and q_E the electronic partition function. Excited states are generally very high in energy and $q_E \sim 1$. The translational, rotational and vibrational partition functions were calculated using established formulas.[36] For the vibrational partition function, the first energy level was chosen as the point of zero energy,[37] and the effect of q_V on the pre–exponential factor is systematically included.

Gaussian 09[38] was used to obtain the moments of inertia and the vibrational frequencies for each species using the following methods.[18] The parameters for the gas-phase partition functions were calculated using the M06-2X density functional[39] and the 6-31G(2df,p) basis set after initial optimisation at the same level of theory. Adsorbed species and transition states were modelled as attached to x Pt atoms as required by their surface coordination. The exchange contribution in M06-2X made convergence difficult and therefore the M06 density

functional[39] was used. A mixed basis set consisting of 6-311G(d,p) for carbon, oxygen and hydrogen and the Stuttgart/Dresden effective core potential[40] for Pt was used. A vibrational frequency analysis followed optimisation at the same level of theory. The TS structure was estimated based on a relaxed potential energy surface (PES) scan along the predicted direction of desorption using 0.02 Å spacing of the adjusted coordinate, starting from the adsorbed species. The position of the TS was determined variationally by minimizing the desorption rate using the canonical variational criterion method,[41] given in Eq. (1),

$$\frac{\delta k^{\infty}}{\delta r^f} = \frac{\delta Q_{\ddagger}}{\delta r^f} = 0 \tag{1}$$

where δr^f is an increase in forward reaction coordinate, $Q_{\ddagger}$ the overall partition function of the TS, and k^{∞} the high–pressure temperature dependent rate constant. The final TS structure contains a single imaginary frequency in the direction of the breaking bond. The M06 and M06-2X functionals were selected on the basis of good performance when compared to reference coupled cluster methods at the CCSD(T)/jun-cc-pVTZ//M06-2X/6-311++G(3df,3pd) level for comparatively complex molecules.[42] The chosen basis sets contain polarisation corrections, while not being prohibitively large. Corrections for hindered rotors were obtained using the Pitzer-Gwinn method[35] (cf. Gaussian 09[38]) as more direct estimates of rotational barriers involve increased complexity.

Comparisons of selected adsorption and desorption rate constants relevant to fuel-lean ethane oxidation are shown in Fig. 1. The reaction rates from the current mechanism have been calculated using VTST for both adsorption and desorption reactions, while the determinations of Vincent et al.[3] rely on sticking coefficients for adsorptions and estimates for desorption reactions. For ethane adsorption, both methods predict an equilibrium on the reactant side. The desorption rates are comparable, while the VTST adsorption rate is considerably slower. For the formyl pathway, the sticking coefficient approach favours adsorption
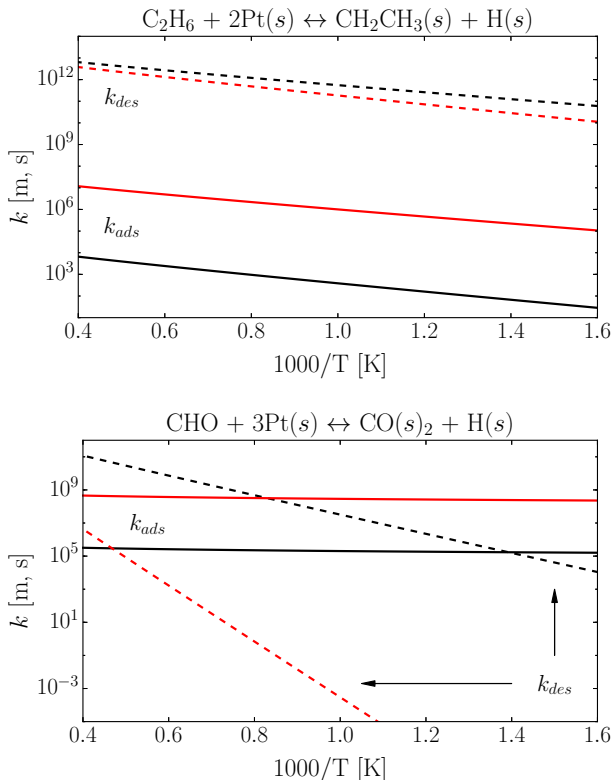
Figure 1: Adsorption (——) and desorption (- -) rate constants of selected pathways in fuel-lean ethane combustion: ethane adsorption (top), formyl adsorption (bottom). Rate parameters from the VTST mechanism (black) and mechanism of Vincent *et al.*[3] (red) are shown. Rate constants in $[ms^{-1}]$ and $[s^{-1}]$ for adsorption and desorption respectively.

over the whole temperature range, while the VTST result suggests that the equilibrium shifts from the product side towards reactants.

Rate constants of selected pathways relevant for fuel-rich ethane oxidation are shown in Fig. 2. Both reaction rates in the mechanism of Vincent *et al.*[3] were highly tuned with the adsorptions having negative temperature dependencies with a sticking coefficient in the form $s_0 = 0.07 \times 300$ K$/T$, based on the value of Hellsing *et al.*[43,44] The rate constants for the associative pathway obtained using the VTST method are in broad agreement with the determinations of Hellsing *et al.*[44] and Vincent *et al.*[3] for the associative adsorption and recombination respectively. For the Eley-Rideal reaction of O_2 with H(s), the VTST determination favours desorption over the whole temperature range, while the determination of Vincent *et al.*[3] favour adsorption at temperatures below 1000 K. The estimated O_2 stick-
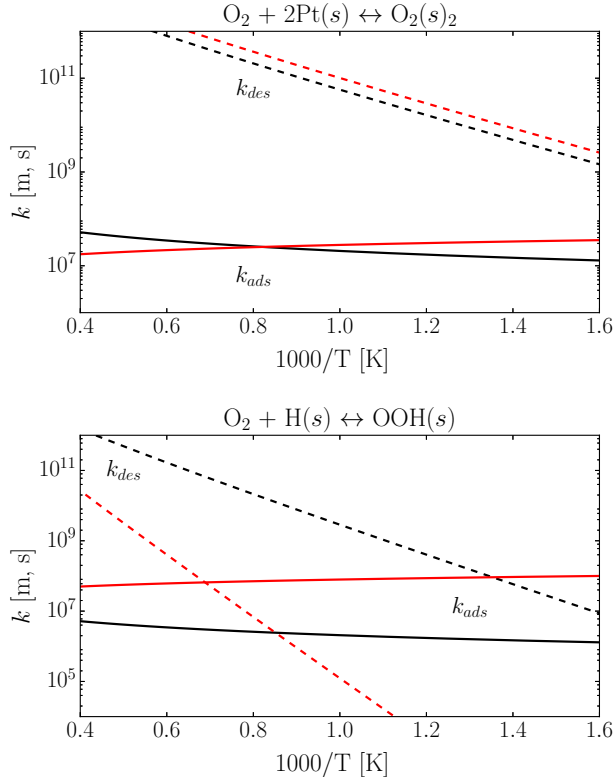
Figure 2: Adsorption (——) and desorption (- -) rate constants of selected pathways in fuel-rich ethane combustion: oxygen associative adsorption (top), oxygen Eley-Rideal reaction with $H(s)$ (bottom). Nomenclature as for Fig. 1.

162 ing coefficient for this Eley-Rideal process leads to a $\sim 35\times$ higher forward rate constant

163 compared to the VTST determination.

Computational methods

165 A purpose-written parabolic FORTRAN code[3,18,45] was used to model the computational

166 domains. A locally refined grid with a geometric scaling and 60 cells in the transverse

167 direction was used for all cases, corresponding to the top half of the experimental domain.

168 The spatial resolution close to the wall and the maximum axial step were set to 1 μm. For

169 the duct reactor, schematically shown in Fig. 3, the temperature at the upper catalytic wall

170 was imposed using the experimental data of Zheng *et al.*[14] For the cases involving catalytic

171 foam reactors, presented in Figs. 4 and 5, only the inlet temperatures are known, therefore

11

172 the thermal balance across the gas-surface interface was calculated according to Eq. (2) as

173 formulated by Coltrin *et al.*[46,47] and used by Vincent *et al.*,[32]

$$\underbrace{\lambda_g \Delta T|_g^W}_{\substack{\text{heat transfer} \\ \text{wall} \to \text{gas}}} - \underbrace{\sum_{i=1}^{N_g} (J_i + \rho Y_i v_s) h_i}_{\substack{\text{enthalpy of diffusing species} \\ \text{at the wall–gas interface}}} = \underbrace{\lambda_w \kappa_1 \Delta T|_b^W}_{\substack{\text{heat transfer} \\ \text{bath} \to \text{wall}}} + \underbrace{\sum_{N_g+1}^{N_g+N_s} R_i M_i h_i}_{\substack{\text{chemical reactions} \\ \text{at the wall}}} \tag{2}$$

174 where λ_g and λ_w are the thermal conductivities of the gas and catalytic wall, respectively.

175 The thermal conductivities were determined in the manner of Vincent *et al.*[3] and $\Delta T|_g^W$

176 is the normal temperature gradient between the wall (catalytic surface) and the gas, while

177 $\Delta T|_b^W$ is the corresponding gradient between the wall and the reactor bath. The imposed

178 reactor bath temperature (T_b) is constant with downstream distance and assigned the case

179 specific values given in Table 2. The specific enthalpy of species i is denoted h_i, while $R_i M_i$

180 is the net production rate of species i. Finally, κ_1 depends on the direction of heat transfer

181 at the bath–wall interface, with $\kappa_1 = 1$ if $\Delta T_b^W \leq 0$, otherwise $\kappa_1 = 0$.

182   Coltrin *et al.*[46] showed that Eq. (2) can be simplified by introducing the coupling of the

183 surface and gas phase chemistries by balancing the species flux at the gas–wall interface with

184 the mass–weighted production rate at the catalytic wall $J_i + \rho Y_i v_s = R_i M_i$, where J_i is the

185 diffusive mass transport, ρ is the density of the fluid, Y_i is the mass fraction of species i and

186 M_i the molecular weight. The summation in the final expression is over all species.

$$\lambda_g \Delta T|_g^W = \lambda_w \kappa_1 \Delta T|_b^W + \sum_{i=1}^{N_g+N_s} R_i M_i h_i \tag{3}$$

187 Raja *et al.*[48] and Sui and Mantzaras[49] noted that for steady state models, as in the present

188 case, the net production rate of surface species is zero and hence performed the summation

189 over gas phase species (N_g) only. The applied Stephan velocity (v_s) is given in Eq. (4).

$$v_s = \frac{1}{\rho} \sum_{i=1}^{N_g} R_i M_i \qquad (4)$$

In the current work, an efficiency factor η_e that accounts for diffusion limitations within the microporous structure of the catalytic wall was applied. An empirical temperature dependency was proposed by Wanker[50] with $\eta_e < 0.5$ for surface temperatures above 800 K. The sensitivity was evaluated using values in the range $0.5 \geq \eta_e \geq 0.1$, corresponding to surface temperatures of 900–1100 K, for the catalytic foam reactors.[32] On metal monolayer surfaces without a microporous structure (e.g. the duct reactor of Zheng *et al.*[14]) the effectiveness factor was set to unity. The efficiency factor is introduced as a multiplier for the reaction rate source terms at the wall, e.g. Eqs. (3) and (4). Depending on the experimental configuration, a radiative heat loss correction is imposed on each computational cell via Eq. (5),

$$T' = T \times \left(1 - \kappa_2 \left(\frac{T}{T_{\mathrm{ad}}} \right)^4 \right) \qquad (5)$$

where T' is the updated temperature, T_{ad} is the adiabatic temperature resulting from the combustion of the inlet mixture, and κ_2 is the radiative heat loss parameter. For the duct reactor data[14] the wall temperature profile is imposed from the experimentally measured values. The experimentally observed profiles should account for non-adiabaticity, accordingly a heat loss correction is not applied. For the catalytic foam reactors[3,12] values in the range of 5–10% were evaluated, corresponding to the suggestion by Vincent *et al.*[3] The impact of κ_2 on gas phase ignition under fuel-lean conditions and on species selectivities and conversion under fuel-rich conditions were also evaluated as discussed below.

Reactant conversion and selectivities

In situ experimental species data for the catalytic foam reactors of Vincent *et al.*[3] and
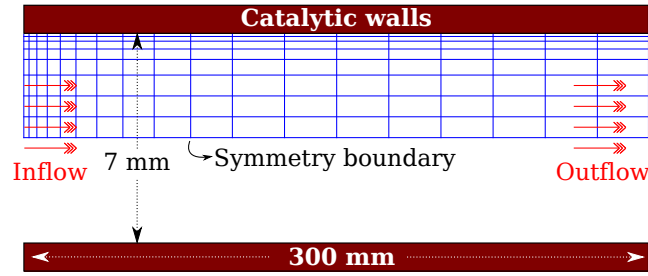
Figure 3: A diagram of the computational domain overlaid over the outline of the experimental configuration of Zheng *et al.*[14]
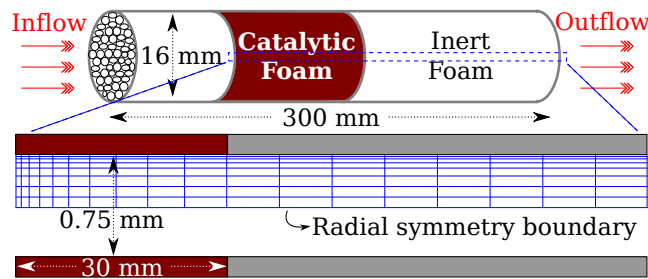

Figure 4: A diagram of the computational domain overlaid over the outline of the experimental configuration of Vincent *et al.*[3] The forward heat shield is excluded from the computational domain.
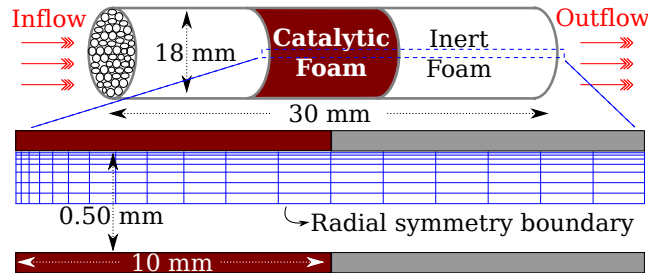

Figure 5: A diagram of the computational domain overlaid over the outline of the experimental configuration of Bodke *et al.*[12] The forward heat shield is excluded from the computational domain.

209 Bodke *et al.*[12] are not available. Validation was hence performed against conversion and
210 species selectivities, experimentally obtained using online gas chromatography of the outlet
211 gas stream. As shown in Figs. 4 and 5, the experimental sampling point is located down-
212 stream of the catalytic and inert alumina sections. While the surface chemistry is confined
213 to the catalytic alumina section, the gas phase chemistry remains active in the inert alumina
214 heat shield, and is hence modelled for the whole length of the foam.

215 Fuel conversion $(\mathcal{C}_f)$ is a measure of the progress of reaction and is calculated as the
216 difference in the radially integrated mass flow of fuel (f) per unit area over all computational
217 cells (N_{cells}) between the inlet (0) and the selected downstream position (d),

$$\mathcal{C}_f = 1 - \frac{f_d}{f_0} \tag{6}$$

$$\text{with: } f_d = \sum_{i=1}^{N_{cells}} \pi \left(r_i^2 - r_{i-1}^2\right) \frac{1}{2} \left((\rho Y_f U)_{i,d} + (\rho Y_f U)_{i-1,d} \right)$$

218 where r_i is the transverse (or radial) position of node i. Additionally, ρ is the fluid density,
219 Y_f is the fuel mass fraction and U is the fluid velocity.

220 The species selectivities are a measure of the distribution of products and in the current
221 work the following definition is applied:

$$\mathcal{S}_s^a = f_{a,s,d} / \left(\left(\sum_{j=1}^{N_g} f_{a,j,d} \right) - f_{a,f,d} \right) \tag{7}$$

$$\text{with: } \quad f_{a,j,d} = \sum_{i=1}^{N_{cells}} \pi \left(r_i^2 - r_{i-1}^2\right) \frac{1}{2} \left((\rho Y'_{a,j} U)_{i,d} + (\rho Y'_{a,j} U)_{i-1,d} \right)$$

$$\text{and: } \quad Y'_{a,j} = Y_j \frac{n_{a,j} M_a}{M_j}$$

222 Therefore, $\mathcal{S}_s^a$ is the ratio of integrated radial mass flux of the selected product s over the
223 fluxes of all products j (excluding the fuel). The mass fractions are scaled by $n_{a,j} M_a$,

224 corresponding to the total weight of atom a in species j. The sum of all selectivities for all
225 atoms sum to unity.

Results and discussion

Fuel-lean conditions

228 Results for ethane oxidation under lean conditions at pressures of 2 and 4 bar (*cf.* E02 and
229 E03 in Table 1) are presented in Fig. 6. Ethane conversion and water production match
230 the experimental data of Zheng *et al.*[14] within 0.4 mol% in the first 50 mm of the reactor.
231 Predictions obtained using the mechanism of Vincent *et al.*[3] are included for comparison.
232 The current VTST mechanism provides more accurate results, especially at 20 and 35 mm
233 downstream. Calculations performed without surface chemistry show no conversion.

234 Figure 7 shows results at higher pressures (*cf.* E04 and E05 in Table 1). The overall
235 behaviour of the system is consistent with the results at lower pressures. However, the
236 agreement between calculations and experimental data is arguably poor for case E04 at 10 bar
237 with C_2H_6 conversion over-predicted close to the catalytic wall. Better agreement is obtained
238 for case E05 at 12 bar, suggesting that the over-prediction for case E04 can not be attributed
239 exclusively to the impact of pressure. Indeed, the differences in surface temperature may
240 exert a significant influence due to the considerable change in the experimental conditions[14]
241 shown in Fig. 8. The simulations carried out by Zheng *et al.*[14] show consistent agreement
242 with reported experimental data for all four cases. The reason for the current discrepancy
243 for case E04 could not be established.

244 Figure 9 shows the transverse profiles of water and ethane for cases E08 and E09 under-
245 going ignition.[14] There is an inconsistency between the predicted and experimental ethane
246 profiles, even at the centerline of the first sampling point in the reactor. The inlet conditions
247 in our simulations were set according to the values published by Zheng *et al.*[14] Despite this
248 inconsistency, the transverse species profiles show qualitative agreement, correctly predicting
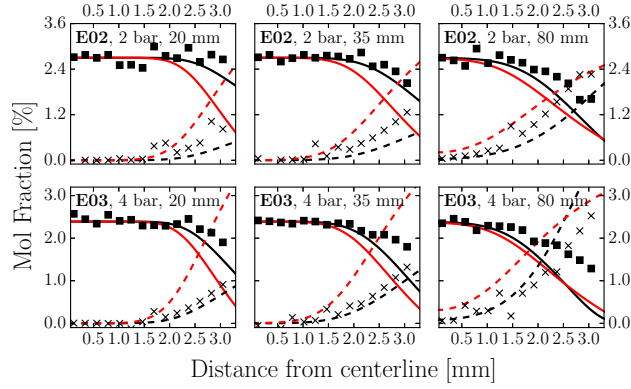
Figure 6: Experimental (symbols) and computational (lines) transverse profiles of major species at different downstream distances in lean ethane combustion cases E02 and E03 at 2 and 4 bar:[14] C_2H_6 (■,—) and H_2O (×,- -). Calculations performed using the VTST (black) and Vincent *et al.*[3] (red) mechanisms are shown.
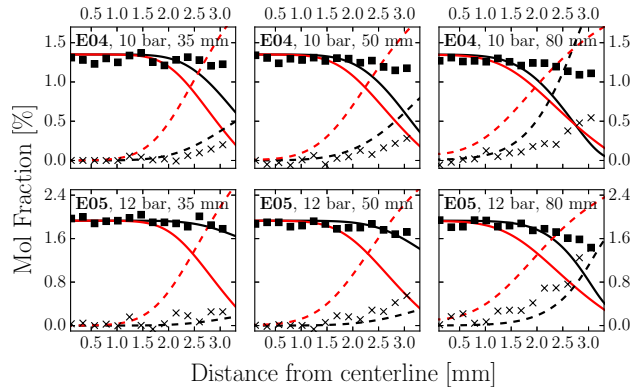

Figure 7: Experimental and computational transverse profiles of major species at different downstream distances in lean ethane combustion cases E04 and E05 at 10 and 12 bar.[14] Symbols and lines as in Fig. 6.
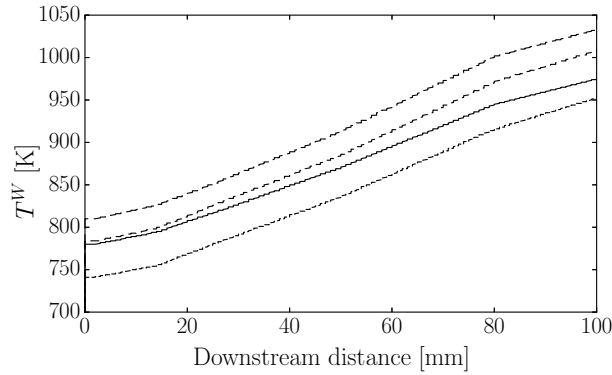

Figure 8: Experimental wall temperatures (T^w) along the reactor obtained from Zheng *et al.*[14] and as imposed for cases E02 (—), E03 (– –), E04 (- - -) and E05 (· · ·) defined in Table 2.
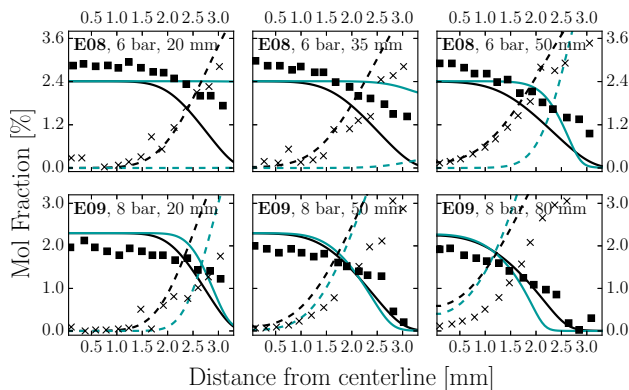
Figure 9: Experimental (symbols) and computational (lines) transverse profiles of major species at different downstream distances in igniting lean ethane cases E08 and E09:[14] C_2H_6 (■,—) and H_2O (×,- -). Calculations performed with the VTST mechanism (black) and with gas phase chemistry only (cyan).
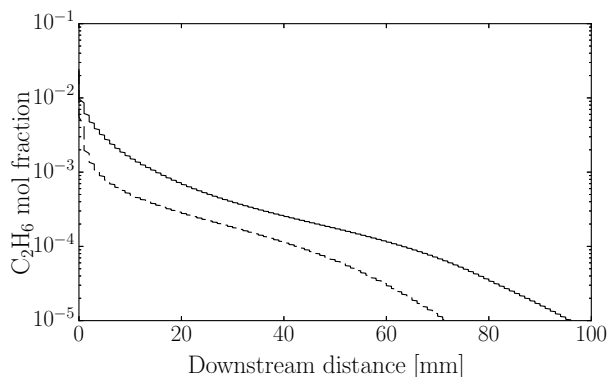

Figure 10: Computed ethane mol fractions adjacent to the catalytic surface along the reactor for cases E08 (—) and E09 (– –) defined in Table 2. The inlet wall temperature for case E08 is 963 K and 1056 K for case E09.
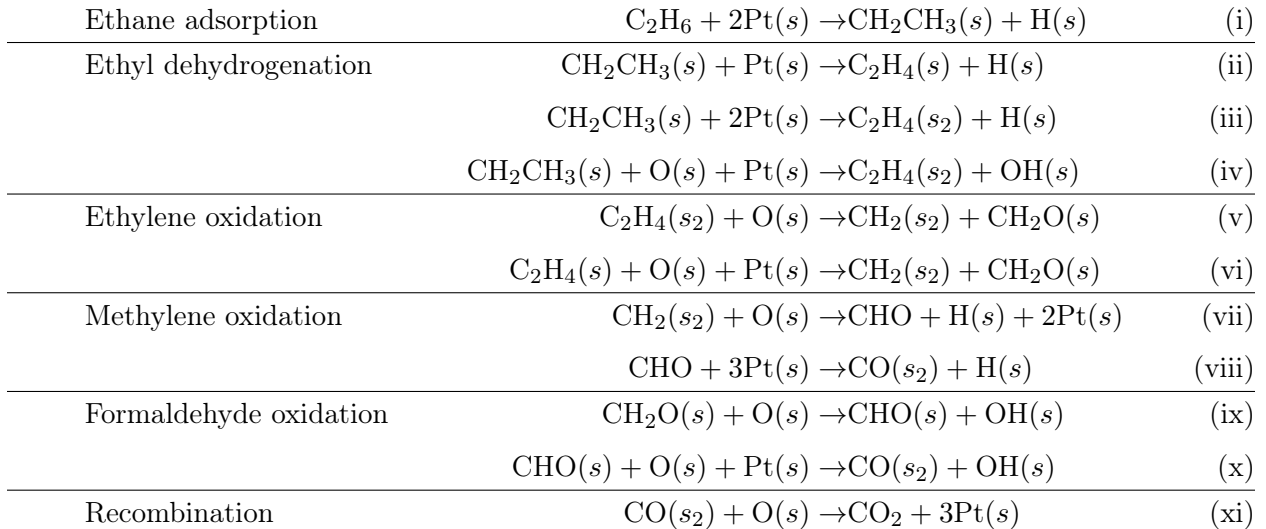
the total ethane conversion close to the catalytic wall at all downstream locations in case E08. When compared to the results obtained with the gas phase chemistry only, the conversion is shown to be mostly surface driven, especially for case E08. The ethane concentration adjacent to the surface is more rapidly reduced for case E09 and hence more affected by limitations in the mass transport as indicated by the evolution of the mol fraction presented in Fig. 10.

18

Effect of heat losses on gas phase ignition

Calculated gas phase ignition distances were 169 and 166 mm for cases E08 and E09 respectively, while the experimental values were reported as 189 and 165 mm. This corresponds to at most a $< 12\%$ under-prediction, which is less than the $\sim 16\%$ obtained by Zheng *et al.*[14] The sensitivity to radiative heat losses was investigated, with $\kappa_2 > 5\%$ resulting in no gas phase ignition. The best agreement with experimental ignition distances (deviation $< 7\%$) was obtained using $\kappa_2 = 3\%$ with no discernible impact on the transverse profiles obtained without radiative heat losses, shown in Fig. 9.

Site and pathway analysis

A surface site analysis shows that $O(s)$ is the major adsorbed species with a site coverage $\theta > 20\%$ at 2 bar and $\theta > 50\%$ at 12 bar at all downstream distances. Other notable species are $OH(s)$ with $\theta > 0.01\%$ in the first half of the reactor at high pressures, and $CO_2(s_2)$ in the latter part of the reactor and at low pressures only. The main product in all studied fuel-lean cases is CO_2. The main pathways involved in the conversion from C_2H_6 to CO_2 are shown below:

Ethane adsorption	$C_2H_6 + 2Pt(s) \rightarrow CH_2CH_3(s) + H(s)$	(i)
Ethyl dehydrogenation	$CH_2CH_3(s) + Pt(s) \rightarrow C_2H_4(s) + H(s)$	(ii)
	$CH_2CH_3(s) + 2Pt(s) \rightarrow C_2H_4(s_2) + H(s)$	(iii)
	$CH_2CH_3(s) + O(s) + Pt(s) \rightarrow C_2H_4(s_2) + OH(s)$	(iv)
Ethylene oxidation	$C_2H_4(s_2) + O(s) \rightarrow CH_2(s_2) + CH_2O(s)$	(v)
	$C_2H_4(s) + O(s) + Pt(s) \rightarrow CH_2(s_2) + CH_2O(s)$	(vi)
Methylene oxidation	$CH_2(s_2) + O(s) \rightarrow CHO + H(s) + 2Pt(s)$	(vii)
	$CHO + 3Pt(s) \rightarrow CO(s_2) + H(s)$	(viii)
Formaldehyde oxidation	$CH_2O(s) + O(s) \rightarrow CHO(s) + OH(s)$	(ix)
	$CHO(s) + O(s) + Pt(s) \rightarrow CO(s_2) + OH(s)$	(x)
Recombination	$CO(s_2) + O(s) \rightarrow CO_2 + 3Pt(s)$	(xi)

Virtually all ethane is adsorbed via the dissociative pathway (i). A comparison of rate constants for this pathway is shown in Fig. 1. Under the current conditions, the direct associative adsorption and Eley-Rideal adsorptions on $O(s)$ and $OH(s)$ are slower than their reverse desorptions. Only around 5% of the ethyl formed via (i) proceeds towards ethylene via the three dehydrogenation pathways (ii–iv). The improved agreement for ethane conversion obtained with the VTST mechanism, shown in Figs. 6 and 7, is a direct result of the lower equilibrium constant for (i) as shown in Fig. 1. The formed ethylene is oxidised in a series of subsequent steps. The first oxidation step is an order of magnitude faster for π-bonded ethylene via pathway (vi) than via di-σ-$C_2H_4(s_2)$. The remaining oxidation steps are fast and do not tend to branch to other products under the studied conditions.

Partial catalytic oxidation

The catalytic foams used in the partial catalytic oxidation experiments contain a microporous structure and the impact of the efficiency factor η_e has to be evaluated. The effect of η_e on ethane and oxygen conversion is shown in Figure 11 for a high inlet velocity case V16 ($U_{in}^{273K} = 6.72$ m/s) where sensitivities are magnified. Vincent et al.[3] used a value of $\eta_e = 0.1$ that was empirically derived for surface temperatures above 1100 K by Wanker.[50] The application of lower values resulted in an under-prediction of the blow–off velocity (~ 6.5 m/s) compared to the experimentally observed value (7.0 m/s). However, the use of a value between 0.2 and 0.4 leads to improved agreement in conversion at high velocities for both mechanisms as shown in Fig. 11. Furthermore, variations in η_e show a minimal influence on selectivities and conversions obtained with the VTST mechanism at inlet velocities U_{in}^{273K} below 5.5 m/s. Therefore, the VTST mechanism will be consistently applied with $\eta_e = 0.4$. The mechanism of Vincent et al.[3] is more sensitive to changes in η_e with a value of 0.3 yielding better results at high inlet velocities at the expense of carbon selectivities at lower inlet velocities as discussed below.

The impact of inlet stoichiometry on conversions and selectivities in partial oxidation has
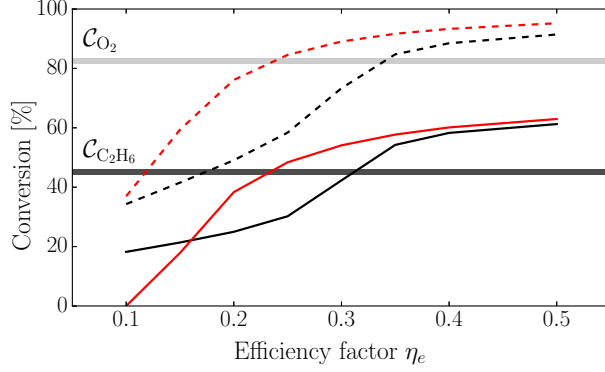
Figure 11: Impact of the efficiency factor η_e at conversion of O_2 (- -) and C_2H_6 (—) at $U_{in}^{273K} = 6.72$ m/s, case V16.[3] The horizontal solid lines represent the corresponding experimental conversions. Simulations carried out using the VTST mechanism (black) and mechanism of Vincent *et al.*[3] (red).
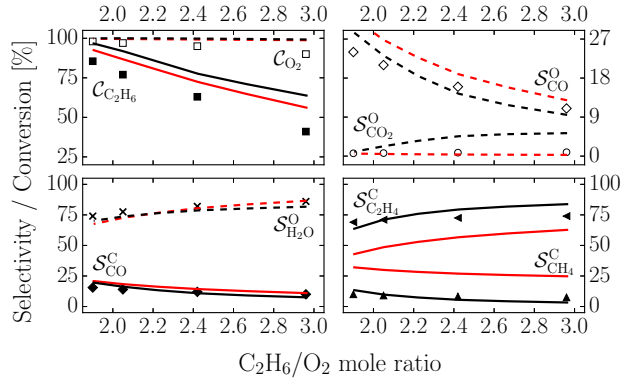

Figure 12: Selectivities and conversions of major species at reactor outlet against inlet composition, cases V07–V12. Experimental data (symbols)[3] and calculations (lines) for: C_2H_6 (■,—) and O_2 (□,- -) conversion, carbon selectivities to C_2H_4 (◄,—), CH_4 (▲,—), CO (♦,—), and oxygen selectivities to H_2O (×,- -), CO_2 (○,- -) and CO (◇,- -). Calculations performed with the VTST mechanism (black) and with the mechanism of Vincent *et al.*[3] (red).

been investigated for four cases from Vincent *et al.*[3] (*cf.* V07–V12, Table 2). The results are presented in Fig. 12. Complete O_2 conversion was predicted in all cases as expected under fuel-rich conditions at long residence times. Ethane conversion is over-predicted by the VTST mechanism by $11 - 20\%$ for cases V12–V07 respectively. The mechanism of Vincent *et al.*[3] shows somewhat better agreement with experimental conversions.

The carbon selectivity to CO is predicted within 2% of the experiments by both mechanisms. The main difference in the results obtained with the two models is in carbon selectivities to C_2H_4 and CH_4. The VTST mechanism yields predictions within 9% of the experiment,
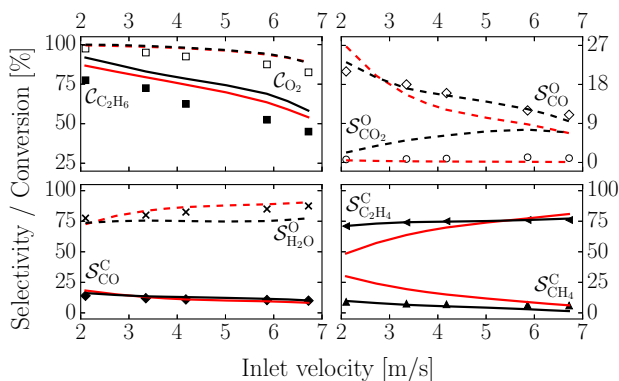
Figure 13: Selectivities and conversions of major species at reactor outlet against inlet velocity, cases V11, V13–V16. Symbols and lines as in Fig. 12.

with the largest discrepancies at high C_2H_6/O_2 ratios. The mechanism of Vincent et al.,[3] applied with $\eta_e = 0.3$ for better agreement at short residence times, as discussed above, produces carbon selectivities with a discrepancy up to 20% compared to the experimental data. This can partly be attributed to the sensitivity towards η_e as the results obtained by Vincent et al.[3] with $\eta_e = 0.1$ are in close agreement with the experimental data. By contrast, the selectivities obtained with the VTST mechanism are not strongly affected by η_e. Oxygen selectivities to H_2O and CO are again equally well predicted by both mechanisms and within 5% of the experimental data. However, the oxygen selectivity to CO_2 is consistently over-predicted by the VTST mechanism, especially at higher C_2H_6/O_2 ratios. The mechanism of Vincent et al.[3] features a highly optimised CO desorption rate and predicts the CO_2 selectivity correctly.

The effect of residence time has been studied by varying the inlet velocity U_{in} for the five cases of Vincent et al.[3] (cf. V11, V13–V16, Table 2). The impact on selectivity and conversion under catalytic partial oxidation conditions is shown in Fig. 13. The mechanism of Vincent et al.[3] shows consistently somewhat better agreement. The decreasing trend of oxygen conversion with increasing velocity is well predicted by both mechanisms. The VTST mechanism predicts all carbon selectivities within 2% of the experimental data at all velocities, outperforming the mechanism of Vincent et al.[3] by a considerable margin. The oxygen selectivity to CO shows similar behaviour with the current approach providing

22

agreement within 2%. The VTST mechanism consistently under-predicts oxygen selectivity to H_2O by $< 10\%$, while CO_2 selectivity is over-predicted by a comparable amount. The mechanism of Vincent et $al.$[3] captures the CO_2 selectivity correctly as discussed below.

The effect of hydrogen co-feed was investigated for the four cases from Bodke et $al.$[12] ($cf.$ B20–B23, Table 2). As details about the catalyst are not available, the site density was set to the bulk platinum value used by Zerkle et $al.$[2] for a related set of experiments. However, when the calculated inlet temperatures of Zerkle et $al.$[2] are applied as boundary conditions, the computed conversions approach unity. Therefore, the inlet temperatures were adjusted to match the experimental conversions with the radiative heat loss factor κ_2 set to 5%. The latter value is at the lower end of the range studied by Vincent et $al.$[3] The obtained outlet gas temperatures were in range of $1099 - 1158$ K with the upper value similar to the reported experimental range of $1178 - 1183$ K.[12] The results are presented in Fig. 14.
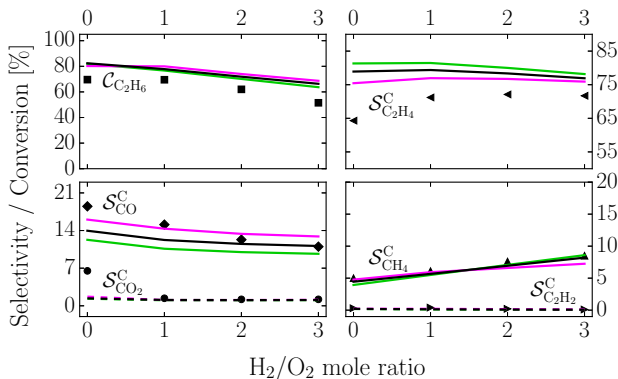

Figure 14: Selectivities and conversions of major species at reactor outlet against H_2/O_2 ratio, cases B20–B23. Experimental data (symbols)[12] and calculations (lines) for: C_2H_6 (■,—) conversion, carbon selectivities to C_2H_4 (◄,—), C_2H_2 (►,- -), CH_4 (▲,—), CO (♦,—) and CO_2 (●,- -). Calculations performed with the VTST mechanism (black), and with O_2 pre–exponentials scaled by a factor of $\times 4$ (green) and $\times 1/4$ (magenta).

The VTST mechanism shows a good quantitative agreement for carbon selectivities to CH_4, C_2H_2, CO and CO_2. Approximately 5% of the experimentally detected products are C_3–C_4 hydrocarbons[12] that are not accounted for in the current C_1–C_2 mechanism. Therefore an over-prediction in C_2H_4 is expected. However, results for case B20 without H_2 co–feed under-predict CO_2 and CO selectivity in favour of C_2H_4, leading to a reduced agreement.
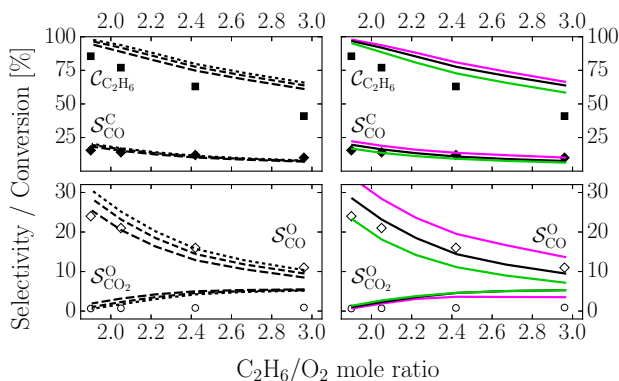
23

Figure 15: Sensitivity of selected parameters to κ_2 (left, $\kappa_2 = 3\%$ ($\cdots$), 7% (- -), 11% ($--$)) and O_2 pre–exponentials (right, ×4 (green),×1 (black),×1/4 (magenta), cases V07–V12: C_2H_6 (■,—) conversion, carbon selectivity to CO (◆,—), oxygen selectivities to CO_2 (○,- -) and CO (◇,- -).

Calculations using the mechanism of Vincent *et al.*[3] show too low conversions, even with increased inlet temperatures.

Sensitivity analysis

The impact of heat losses was further investigated via the sensitivity to the radiative heat loss factor κ_2 for selected cases from Vincent *et al.*[3] (*cf.* V07–V12, Table 2). The system shows a strong correlation between conversion and κ_2, as shown in Fig. 15 (left). Simulations with a higher radiative heat loss show lower overall conversion and lower selectivities to CO. Increasing κ_2 to 11% results in an improved agreement with experimental data.

The sensitivity to various parameters in the VTST based framework has also been investigated. Excluding hindered rotor corrections from the vibrational partition functions has no visible impact on results. The system exhibits a large sensitivity to the O_2 adsorption and desorption rates, as shown by the coloured lines in Fig. 15 (right) for the cases of Vincent *et al.*[3] and Fig. 14 for the cases of Bodke *et al.*,[12] with a profound effect on CO selectivities in all cases. A reduction of the reaction rates by a factor of ×1/4 leads to 3% higher oxygen and 1% higher carbon selectivity to CO. The oxygen selectivity to H_2O and carbon selectivity to C_2H_4 also correlate with the studied rates. Additionally, the reduction of the pre–exponential terms lead to a considerable under-prediction of the blow–off velocity

[357] (~ 5.0 m/s compared to the experimental value of 7.0 m/s[3]). Notably, the O_2 adsorption

[358] rates used in the mechanism of Vincent *et al.*[3] are highly tuned, with a negative tempera-

[359] ture dependency and a sticking coefficient of 0.07 at 300 K.[44,51] The current, systematically

[360] derived O_2 adsorption rate constants were presented in Fig. 2. A reduction of the associative

[361] adsorption rate (see Fig. 2 (top)) by a factor of $\times 1/4$ leads to a closer agreement with the

[362] sticking coefficient rate constants in the mechanism of Vincent *et al.*[3] at temperatures above

[363] 1200 K.

[364] The sensitivity to a $\pm 20\%$ change in heats of adsorption of all species has also been

[365] investigated. The most profound effects are observed by variations in Q_{CO}, especially for

[366] the cases of Vincent *et al.*,[3] with higher values leading to higher CO and lower CO_2 selec-

[367] tivity. The sensitivity towards this parameter has been previously highlighted.[2,3,16,18] In the

[368] mechanisms of Zerkle *et al.*[2] and Vincent *et al.*,[3] the CO desorption pre-exponential was

[369] optimised, while in the VTST mechanism the pre-exponential was not adjusted. The result

[370] suggests that for this channel, reaction rate optimisation and/or detailed DFT studies would

[371] be beneficial. The value of Q_{OH} has a large impact on the C_2H_4, CO_2 and CH_4 selectivity

[372] for the cases of Bodke *et al.*[12] However, variations in Q_{OH} require an adjustment of inlet

[373] temperature from the currently imposed measured values. Additionally, modest effects on

[374] CO and CO_2 selectivities ($\approx 1\%$) are observed by a variation in $Q_{C_2H_4}$, Q_{CH_4}, and Q_{CH_3},

[375] especially at higher C_2H_6/O_2 ratios. The results are not sensitive to heats of adsorption of

[376] C_2H_6, C_2H_2, CHO, O_2, H_2 and CO_2.

Conclusions

[378] The updated VTST based reaction class based framework of Kraus and Lindstedt[18] has been

[379] applied to the case of partial ethane oxidation and combustion over Pt. Transverse species

[380] profiles for the latter cases of Zheng *et al.*[14] are well predicted, generally within 0.4 mol%,

[381] providing an improvement over the collision theory based mechanism of Vincent *et al.*[3]

Ignition distances for the studied cases are predicted within 7% of the experimental data with heat losses of 3% and compare favourably with calculations by Zheng *et al.*[14]

For the partial catalytic oxidation of ethane, the VTST based mechanism correctly predicts the impact of C_2H_6/O_2 ratio and inlet velocity on selectivities to major species with the exception of CO_2, which is over-predicted. Ethane conversion is also somewhat high, especially at very rich conditions or for inlet velocities above 5 m/s. However, the VTST mechanism compares favourably with the mechanism of Vincent *et al.*[3] under other conditions and without the need for reaction rate parameter optimisation. The updated mechanism was also validated against the experimental data of Bodke *et al.*[12] and shows good overall performance for cases with H_2 co–feed. A pathway analysis was performed and the O_2 adsorption and desorption rate found to be a sensitive parameter. A reduction by a factor of 1/4 was found to lead to better agreement for selected cases presented by Vincent *et al.*[3] and for all cases of Bodke *et al.*[12] Other sensitive parameters include the heats of adsorption of OH and CO (Q_{OH}, Q_{CO}) as also discussed by Kraus and Lindstedt.[18]

Overall, the current VTST based mechanism provides improved generality compared to the mechanism of Vincent *et al.*[3] by being applicable to both fuel rich and lean conditions in addition to the previously reported cases of hydrogen and syngas combustion.[18] Furthermore, the method does not require the separate determination or estimation of sticking coefficients. That latter is major advantage for systems where experimental data is scarce.

Acknowledgements

References

(1) Bodke, A. S.; Olschki, D. A.; Schmidt, L. D.; Ranzi, E. *Science* **1999**, *285*, 712–715.

(2) Zerkle, D. K.; Allendorf, M. D.; Wolf, M.; Deutschmann, O. *J. Catal.* **2000**, *196*, 18–39.

(3) Vincent, R.; Lindstedt, R. P.; Malik, N.; Reid, I.; Messenger, B. *J. Catal.* **2008**, *260*, 37–64.

(4) Horn, R.; Williams, K. A.; Degenstein, N. J.; Bitsch-Larsen, A.; Dalle Nogare, D.; Tupy, S. A.; Schmidt, L. D. *J. Catal.* **2007**, *249*, 380–393.

(5) Appel, C.; Mantzaras, J.; Schaeren, R.; Bombach, R.; Inauen, A.; Tylli, N. N.; Wolf, M.; Griffin, T.; Winkler, D.; Carroni, R. *Proc. Combust. Inst.* **2005**, *30*, 2509–2517.

(6) Cortright, R. D.; Watwe, R. M.; Spiewak, B. E.; Dumesic, J. A. *Catal. Today* **1999**, *53*, 395–406.

(7) Cortright, R. D.; Watwe, R. M.; Dumesic, J. A. *J. Mol. Catal. A Chem.* **2000**, *163*, 91–103.

(8) Watwe, R. *J. Catal.* **1998**, *180*, 184–193.

(9) Salciccioli, M.; Chen, Y.; Vlachos, D. G. *Ind. Eng. Chem. Res.* **2011**, *50*, 28–40.

(10) Chen, Y.; Vlachos, D. G. *J. Phys. Chem. C* **2010**, *114*, 4973–4982.

(11) Bodke, A. S.; Bharadwaj, S. S.; Schmidt, L. D. **1998**, *149*, 138–149.

(12) Bodke, A. S.; Henning, D.; Schimdt, L. D.; Bharadwaj, S. S.; Maj, J. J.; Siddall, J. *J. Catal.* **2000**, *191*, 62–74.

(13) Vincent, R. S.; Lindstedt, R. P.; Malik, N. A.; Reid, I. A. B.; Messenger, B. E. *Proc. Combust. Inst.* **2011**, *33*, 1809–1817.

(14) Zheng, X.; Mantzaras, J.; Bombach, R. *Proc. Combust. Inst.* **2013**, *34*, 2279–2287.

(15) Deutschmann, O.; Maier, L. I.; Riedel, U.; Stroemman, A. H.; Dibble, R. W. *Catal. Today* **2000**, *59*, 141–150.

(16) Shustorovich, E.; Sellers, H. *Surf. Sci. Rep.* **1998**, *31*, 5–119.

(17) Warnatz, J. *Proc. Combust. Inst.* **1992**, *24*, 553–579.

(18) Kraus, P.; Lindstedt, R. P. *Proc. Combust. Inst.* **2016**, *36*.

(19) Reid, I. A. B.; Robinson, C.; Smith, D. B. *Proc. Combust. Inst.* **1985**, *20*, 1833–1843.

(20) Lindstedt, R. P.; Skevis, G. *Proc. Combust. Inst.* **2000**, *28*, 1801–1807.

(21) Lindstedt, R. P.; Meyer, M. P. *Proc. Combust. Inst.* **2002**, *29*, 1395–1402.

(22) Cerru, F. G.; Kronenburg, A.; Lindstedt, R. P. *Combust. Flame* **2006**, *146*, 437–455.

(23) Shustorovich, E. *Adv. Catal.* **1990**, *37*, 101–163.

(24) Olivera, P. P.; Patrito, E. M.; Sellers, H. *Surf. Sci.* **1995**, *327*, 330–357.

(25) Fujimoto, G. T.; Selwyn, G. S.; Keiser, J. T.; Lin, M. C. *J. Phys. Chem.* **1983**, *87*, 1906–1910.

(26) Anton, A. B.; Cadogan, D. C. *Surf. Sci. Lett.* **1990**, *239*, L548–560.

(27) Kuz'min, I. V.; Zeigarnik, A. V. *Kinet. Catal.* **2004**, *45*, 561–568.

(28) Podkolzin, S. G.; Alcalá, R.; Dumesic, J. A. *J. Mol. Catal. A Chem.* **2004**, *218*, 217–227.

(29) Shustorovich, E. *Surf. Sci. Lett.* **1986**, *176*, L863–L872.

(30) Brass, S. G.; Ehrlich, G. *Surf. Sci.* **1987**, *187*, 21–35.

(31) Green, W. H.; Allen, J. W.; Buesser, B. A.; Ashcraft, R. W.; Beran, G. J. RMG. 2013; http://rmg.sourceforge.net.

(32) Vincent, R. S. Detailed modelling of catalytic chemistry in short contact time reactors. Ph.D. thesis, Imperial College London, 2008.

(33) Carr, R. W. *Compr. Chem. Kinet.*; 2007; Vol. 42; pp 43–99.

(34) Ariya, P. A.; Skov, H.; Grage, M. M.-L.; Goodsite, M. E. *Adv. Quantum Chem.*; 2008; Vol. 55; pp 43–55.

(35) Pitzer, K. S.; Gwinn, W. D. *J. Chem. Phys.* **1942**, *10*, 428–440.

(36) Dumesic, J. A. *The Microkinetics of heterogeneous catalysis*; ACS professional reference book; American Chemical Society, 1993.

(37) Ochterski, J. W. *Thermochemistry in Gaussian*; 2000; pp 1–19.

(38) Frisch, M. J. et al. Gaussian 09 Revision D.01. 2009; `www.gaussian.com`.

(39) Zhao, Y.; Truhlar, D. G. *Theor. Chem. Acc.* **2008**, *120*, 215–241.

(40) Andrae, D.; Häußermann, U.; Dolg, M.; Stoll, H.; Preuß, H. *Theor. Chim. Acta* **1990**, *77*, 123–141.

(41) Hase, W. L. *Acc. Chem. Res.* **1983**, *16*, 258–264.

(42) Robinson, R. K.; Lindstedt, R. P. *Combust. Flame* **2013**, *160*, 2642–2653.

(43) Hellsing, B.; Kasemo, B.; Ljungström, S.; Rosén, A.; Wahnström, T. *Surf. Sci.* **1987**, *189-190*, 851–860.

(44) Hellsing, B.; Kasemo, B.; Zhdanov, V. P. *J. Catal.* **1991**, *132*, 210–228.

(45) Leung, K. M.; Lindstedt, R. P. *Combust. Flame* **1995**, *102*, 129–160.

(46) Coltrin, M. E.; Kee, R. J.; Rupley, F. M. SURFACE CHEMKIN (Version 4.0): A Fortran package for analyzing heterogeneous chemical kinetics at a solid-surface – gas-phase interface. SANDIA Report, SAND90-8003B, UC-401, July 1991, `http://www.osti.gov/scitech/servlets/purl/6128661`.

(47) Coltrin, M. E.; Kee, R. J.; Rupley, F. M. *Int. J. Chem. Kinet.* **1991**, *23*, 1111–1128.

473 (48) Raja, L. L.; Kee, R. J.; Petzold, L. R. *Proc. Combust. Inst.* **1998**, *27*, 2249–2257.

474 (49) Sui, R.; Mantzaras, J. *Combust. Flame* **2016**, *173*, 370–386.

475 (50) Wanker, R. *Chem. Eng. Sci.* **2000**, *55*, 4709–4718.

476 (51) Rinnemo, M.; Deutschmann, O.; Behrendt, F.; Kasemo, B. *Combust. Flame* **1997**, *111*,
477 312–326.